Dynamics in photosynthetic transient complexes studied by paramagnetic NMR spectroscopy

Scanu, S.

Chapter II

The complex of cytochrome *f* and plastocyanin from *Nostoc sp*. PCC 7119 is highly dynamic

Abstract

Cyt *f* and Pc form a highly transient complex as part of the photosynthetic redox chain. The complex from *Nostoc sp.* PCC 7119 was studied with NMR relaxation spectroscopy with the aim to determine the orientation of Pc relative to Cyt *f*. Chemical shift perturbations analysis showed that the presence of spin labels on the surface of Cyt *f* does not significantly affect the binding of Pc. The paramagnetic relaxation enhancement results are not in agreement with a single orientation of Pc indicating that multiple orientations must occur and suggesting that the encounter state represents a large fraction of the complex.

Introduction

The concept of protein-protein complex formation is evolving towards a view in which an encounter state is in dynamic equilibrium with the well-defined, specific complex.
The initial approach of the proteins and subsequent formation of the encounter state are thought to be mainly driven by long-range electrostatic forces, whereas the well-defined complex is stabilized by short-range interactions, like hydrogen bonds and van der Waals forces.[21] Until recently it was not possible to characterize the encounter state experimentally. However, several existing methods have been adapted for this purpose, like double-mutant cycles combined with measurements of association kinetics,[111] flash photolysis kinetics[112] and PRE NMR spectroscopy.[84,113] The first complex of ET proteins characterized by this approach was that of cytochrome *c* (Cyt *c*) and cytochrome *c* peroxidase (CcP). The solution structure of this complex has been determined by PRE NMR[114] showing that Cyt *c* has the same orientation within the complex as in the crystal structure.[110] At the same time the PRE data provided evidence for dynamics within the complex, suggesting that the encounter complex was significantly populated. In combination with Monte Carlo docking the encounter state could be visualized and its fraction established to be 30%.[28] This approach opens the door for the characterization of the encounter state in other transient redox complexes.[20]
Pc and Cyt *f* form a redox complex in oxygenic photosynthesis. Pc shuttles electrons from Cyt *f* of the b_6f complex to P700 in PSI. The surface charge properties of Pc and Cyt *f*, which vary significantly between the different species, influence the relative orientation of the interaction partners in the well-defined complex. Two general orientations have been described, dubbed "side-on" and "head-on". The "side-on" orientation has been observed in plant complexes.[115,116] The plant proteins exhibit a favourable electrostatic interaction due to the presence of negatively and positively charged patches of amino acids on Pc and Cyt *f*, respectively. The patches align the long sides of Pc and Cyt *f*, enabling rapid ET by bringing a hydrophobic patch on Pc close to the haem in Cyt *f*.[115] In the cyanobacterial complex from *Phormidium laminosum*, Pc approaches Cyt *f* "head-on".[54] Within the complex, Pc is oriented perpendicular to the haem plane and only its hydrophobic patch participates in the interaction. Electrostatics play a smaller role in *Phormidium* than in plants,[117] although kinetics studies[118,119] suggested charge interactions contribute to the formation of the encounter state. In the cyanobacterial complexes from *Nostoc sp.* PCC 7119[120] and *Prochlorothrix hollandica,*[32] where the charge distribution is reversed compared to that in plants, again the "side-on" orientation was observed. The solution models of the complexes have been determined by rigid-body docking of the structures of the individual proteins on the basis of binding CSPs and intermolecular PCSs of Pc nuclei induced by the paramagnetic, oxidized iron of Cyt *f*.[115] In the case of the *Nostoc* complex site-directed mutagenesis studies investigating the influence of charges on the kinetics of the complex formation, highlighted how the loss of either positive charges on Pc[121] or negative charges on Cyt *f*[122] causes a decreased association rate constant. It could be shown that for Pc several

charges are pivotal for the interaction.[121,122] On the other hand, the charges on Cyt *f* are more spread over the surface and no "hot spots" were identified either in *Nostoc*[122] or *Phormidium,*[119] suggesting that the encounter complex may have an important role in these complexes. To obtain independent restraints for the refinement of the well-defined state and to establish whether the encounter state is significantly populated, the Pc-Cyt *f* complex from *Nostoc* was studied by PRE NMR spectroscopy. The data cannot be described by the structure determined by pseudocontact shifts alone, or indeed by any single structure, indicating that the encounter ensemble must represent quite a significant fraction of the complex.

Experimental section

Protein production and purification

The plasmid pEAP-WT containing the gene encoding *Nostoc sp.* PCC 7119 Pc was kindly provided by Prof. Dr. Miguel A. De la Rosa (University of Seville). The leader sequence, consisting of 34 amino acids, was removed in order to achieve cytoplasmic expression of the mature Pc (as defined in Uni*P*rot entry O52830). An N-terminal Met residue was added to initiate translation. This construct was obtained by subcloning with PCR, using the following primers according to the Cloning Standard Protocol (Qiagen®).

FWD: 5'- ctgtgcaa**ccatgg**aaacatacacagtaaaactaggtagcg -3'
REV: 5' -ctgtgcaa**ctcgag**ttagccggcgacagtgattttacc – 3'.

The restriction site for *Nco*I and *Xho*I were introduced in the forward and reverse primers, respectively, and are indicated with bold letters. The former comprises the ATG codon for initiation Met residue. The amplified gene and the vector pET28a were doubly digested with these enzymes before the ligation step. The construct (pSS01) was verified by DNA sequencing.
Uniformly ^{15}N-labeled Pc was produced in *E. coli* BL21 freshly transformed with pSS01. A single colony was inoculated in lysogeny broth (LB, 2 mL) with kanamycin (25 mg/L) and cultured until the OD_{600} reached 0.6. Fifty microlitres were used to inoculate ^{15}N M9 minimal medium (50 mL) with $^{15}NH_4Cl$ (0.3 g/L) as only source of nitrogen and kanamycin (25 mg/L), which was incubated overnight. Five millilitres of culture were transferred into ^{15}N minimal medium (0.5 L), and incubated until the OD_{600} reached 0.6. All cultures were incubated at 37°C, 250 rpm. Then, the expression of the gene encoding Pc was induced with isopropyl β-D-1-thiogalactopyranoside (IPTG, 1 mM) and the temperature was decreased to 22°C. The cells were harvested after 20 hours by centrifugation at 6400 g for 20 min at 4°C. The pellet was resuspended in sodium phosphate (NaP_i, 10 mL, 1 mM, pH 7). Phenylmethylsulfonyl fluoride (PMSF, 1 mM), DNase (0.2 mg/ mL) and $ZnCl_2$ (250 μM) were added. Cells were lysed using a French Press. The cell lysate was cleared by ultracentrifugation at 210000 g for 30 min at 4°C and the supernatant was dialyzed overnight against NaP_i (1 mM, pH 7), $ZnCl_2$ (25 μM). The solution was

cleared by ultracentrifugation and loaded onto a carboxymethyl (CM) cellulose Sephadex C-50 column (GE Healthcare) equilibrated with the same buffer, in the absence of zinc. The elution was carried out with a gradient of NaP_i (1-25 mM, pH 7). The fractions containing Pc were loaded once again on the same column and eluted under the same conditions. The concentration of the protein was determined by absorbance spectroscopy using ε_{280} = 5 $mM^{-1}cm^{-1}$. The yield of pure protein was (10 mg/L) of culture. The absence of Cu was verified by UV-vis spectroscopy by the absence of the characteristic band at 595 nm under oxidizing conditions. The presence of Zn was verified by atomic absorption spectroscopy.

The pEAF-WT plasmid, containing the gene of the soluble domain (residue 1-254) of *Nostoc sp.* PCC7119 Cyf *f* was kindly provided by Prof. Dr. Miguel A. De la Rosa (University of Seville). The pEAF-WT plasmid was used as template to obtain Cyt *f* mutants. The mutations to cysteine were introduced by using the QuikChange Site-Directed Mutagenesis kit (Stratagene). The primers used for the mutations at the positions N71 and Q104 were described before.[123] The primers employed for the introduction of a cysteine at the position S192 were:

FWD: 5' –ggcgaagatggttgcgttaaatatttagt**c**gacatc-3'
REV: 5' – gatgtc**g**actaaatatttaacgcaaccatcttcgcc-3'

For S192C a silent mutation (bold) was designed to introduce an extra Sal I restriction site, located close to the *3'* end of the forward primer. The codon-changing mutations are shown underlined. The mutant genes were verified by DNA sequencing.

Truncated Cyt *f* was produced in *E. coli* MV1190 (Δ(*lac-pro*AB), *thi*, *sup*E, Δ(*srl-rec*A) 306::Tn10 (tet^r) [F′:*tra*D36, *pro*AB+, $lacI^qZ\Delta M15$]), transformed with pEAF-WT or mutant plasmids and co-transformed with pEC86,[124] which contains a cassette for *c*-type cytochrome overexpression. A single colony of co-transformed *E.Coli* MV1190 was inoculated into LB (50 mL) containing chloramphenicol (20 mg/L) and ampicillin (100 mg/L), and cultured at 37°C, 250 rpm for 5-6 h. Five millilitres of culture were used to inoculate LB (1.7 L) with the same antibiotics in a 2 L Erlenmeyer flask. The culture was incubated at 25°C, 150 rpm for 20 h before further addition of chloramphenicol (20 mg/L) and ampicillin (100 mg/L). After again two hours incubation, gene expression was induced with IPTG (1 mM). The cells were harvested 96 hours after induction. The purification of the protein was performed as previously reported.[121] Dithiothreitol (DTT, 3 mM) was added to the buffers during the purification to prevent the dimerisation of the cysteine mutants. It was removed immediately before spin labelling by buffer exchange on a PD10 column (GE Healthcare), equilibrated with 2-(*N*-morpholino) ethanesulfonic acid (MES) buffer (20 mM, pH 6). The ferrous form of the Cyf *f* cysteine mutants was used for the attachment of (1-Acetoxy-2,2,5,5-tetramethyl-δ-3-pyrroline-3-methyl) methanethiosulfonate (MTS) or (1-Oxyl-2,2,5,5-tetramethyl-δ-3-pyrroline-3-methyl) methanethiosulfonate (MTSL), with a protein concentration ranging from 20 to 80 μM. A 20-fold molar excess of MTS(L) was added and the solution was incubated for one hour on ice. A 100-fold molar excess of $K_3[Fe(CN)_6]$ was then added to oxidize the haem iron and prevent reduction of the nitroxyl group or the

disulphide bridge by the ferrous haem.
The sample was concentrated by ultrafiltration to a volume of 0.5 mL and loaded on a Superdex75 gel filtration column (GE Healthcare) equilibrated with MES buffer (20 mM, pH 6). The fractions containing MTS(L)-Cyt *f* were concentrated and the buffer was exchanged by ultrafiltration to MES (20 mM, pH 6), $K_3[Fe(CN)_6]$ (0.5 mM). The attachment of the spin label was verified by mass spectrometry and the presence of the nitroxyl radical was checked by EPR spectroscopy. The concentration of the protein was determined by absorbance spectroscopy using $\varepsilon_{556} = 31.5\ mM^{-1}cm^{-1}$ for ferrous Cyt *f*.

NMR experiments

All NMR samples contained MES (20 mM, pH 6) and 6% D_2O for lock. Cyt *f* was kept in the ferric state by addition of $K_3[Fe(CN)_6]$ (50 μM). The pH of the sample was adjusted with small aliquots of HCl (0.5 M) and NaOH (0.5 M). For the chemical shifts perturbation experiments Cyt *f* was titrated into Zn-substituted ^{15}N Pc (50 μM). Spectra were recorded at multiple Cyt *f*:Pc molar ratios (0.1, 0.2, 0.4, 0.6, 0.8, 1.0, 2.5, 5.0). Samples for PRE measurements contained Cyt *f* (66 μM) labelled with either MTS or MTSL and Zn-substituted ^{15}N Pc (200 μM). All NMR spectra were recorded at 298 K on a Bruker Avance III 600 MHz spectrometer equipped with a TCI-Z-GRAD CryoProbe. The ^{1}H-^{15}N HSQC spectra were acquired with 1024 and 80 complex points in the direct and indirect dimensions, respectively.

Data analysis

The NMR spectra were processed with NmrPipe[125] and analyzed with CcpNMR.[126] The assignments for the Zn ^{15}N Pc amide resonances were kindly provided by Dr. Mathias A. S. Hass. The assignments for the residues K6 and V29 could not be made because of overlap of the corresponding peaks in the HSQC spectra. The chemical shift perturbations ($\Delta\delta_{bind}$) of Pc resonances due to complex formation with Cyt *f* were plotted against the molar ratio Cyt *f*/Pc (*R*). Note that the perturbations include both the effect of binding and the PCS caused by the ferric haem iron in all samples. The entire perturbation was used in the analysis and the PCS was not used separately in this study.
The corresponding titration curves were fitted in OriginLab 8.1 (www.originlab.com) with a non-linear least square fit to a 1:1 binding model, Equation 2.1.[127]

$$\Delta\delta_{bind} = \frac{1}{2}\Delta\delta^{\infty}_{bind}\left[A - \sqrt{A^2 - 4R}\right] \quad A = 1 + R + \frac{P_0R + C_0}{P_0C_0K_a} \qquad (2.1)$$

Where $\Delta\delta^{\infty}_{bind}$ is the chemical shift perturbation for 100% bound Pc, P_0 is the starting concentration of Pc and C_0 is the stock concentration of Cyt *f*. A global fit with a single binding constant ($K_a = K_D^{-1}$) for the data of several residues was used. The binding maps were obtained by extrapolation of the $\Delta\delta_{bind}$ values at the 5:1 Cytf:Pc molar ratio of all residues to 100% bound Pc using the K_D. These

extrapolated perturbations were averaged for the nitrogen ($\Delta\delta_N$) and hydrogen ($\Delta\delta_H$) atoms of each amide, yielding $\Delta\delta_{avg}$, according to Equation 2.2:

$$\Delta\delta_{avg} = \sqrt{\frac{(\Delta\delta_N/5)^2 + \Delta\delta_H{}^2}{2}} \qquad (2.2)$$

The PREs were determined according to the procedure of Battiste and Wagner.[128] The intensity ratio I_p/I_d of the Pc resonances in the presence of MTSL-Cyt *f* (I_p) and MTS-Cyt *f* (I_d) were normalized by dividing them by the average value of the ten largest I_p/I_d values (1.13 for N71C and Q104C; 1.06 for S192C). The PRE (Γ_2) values were calculated according to the formula:

$$\frac{I_p}{I_d} = \frac{R_{2d}\exp(-\Gamma_2 t)}{R_{2d} + \Gamma_2} \qquad (2.3)$$

The transverse relaxation rates in the diamagnetic sample (R_{2d}) were calculated from the linewidth at half height obtained from a Lorentzian peak fit in the direct dimension, by using MestReC (www.metsrelab.com). The symbol *t* denotes the time for transverse relaxation during the pulse sequence (9 ms).

Structure calculations

The PREs were converted into distances for structure calculations using Equation 2.4:

$$r = \sqrt[6]{\frac{\gamma^2 g^2 \beta^2}{\Gamma_2}\left(4\tau_c + \frac{3\tau_c}{1+\omega_h^2\tau_c^2}\right)} \qquad (2.4)$$

Where *r* is the distance between the oxygen atom of MTSL and the Pc amide proton, γ is the proton gyromagnetic ratio, *g* is the electronic g-factor, β is the Bohr magneton, ω_h is the Larmor frequency of the proton and τ_c is the rotational correlation time of the MTSL oxygen-proton vector. τ_c was taken to be 30 ns on the basis of the HYDRONMR[129] prediction of the rotational correlation time for the Pc-Cyt *f* complex. In the docking procedure this value gave rise to the lowest energy structures in comparison with τ_c values of 20 ns, 25 ns, 35 ns and 40 ns.
Three classes of restraints were included in the calculations: 1) For residues with I_p/I_d ratios < 0.1, including those for which the resonances disappeared from the spectrum, the upper bound distance limit was set to 14 Å; 2) For residues with I_p/I_d ratios > 0.95 the lower bound distance limit was set to 22 Å; 3) For residues with I_p/I_d ratios between 0.1 and 0.95 the distances calculated with equation 2.4 were used with upper and lower bounds of 4 Å. The structure calculations were done in Xplor-NIH.[130] Cyt *f* and Pc were both considered as rigid bodies, the coordinates of Cyt *f* were fixed, and Pc was allowed to move in a restrained rigid-body molecular dynamics calculation. The structure of the soluble domain of Cyt *f* used

for the calculation was taken from the crystal structure of the b_6f complex from *Nostoc* sp. PCC 7120, PDB entry 2ZT9.[131] The amino acidic sequences of Cyt *f* from *Nostoc* sp. PCC 7120 and sp. PCC 7119 are identical. Mutations and spin labels were modelled on the structure of Cyt *f*. Four conformations were used to represent the mobility of the spin label,[132] and the distances to the Pc nuclei were r^{-6} averaged for these MTSL conformers. The structure of Pc was taken from PDB entry 2CJ3. At each cycle Pc was placed at a random position and the protein was docked as rigid body only on the basis of the experimental restraints and a van der Waals repel function to avoid steric collision. Two hundred approaches were performed, yielding 155 structures with restraint energies below a given threshold. The ten lowest energy structures were selected and they showed an average r.m.s.d. difference of 0.83 Å to the mean structure.

Results and discussion

Characterisation of MTS-tagged Cyt *f*

To study the complex of Cyt *f* and Pc with PRE NMR spectroscopy, three sites for probe attachment were selected. The positions of the mutations were designed on the basis of the solution structure of the wild type complex determined by NMR spectroscopy on the basis of PCS and chemical shift perturbations.[120] The rationale of the work followed that of Volkov et al.[114] for the complex CcP and Cyt *c*, i.e. to obtain constraints for structure determination and improve the precision of the solution structure that was based on PCS. The residues that were mutated to cysteine were N71, Q104, and S192, which are located around the Pc binding site (Figure 2.1). In order to preserve the overall electrostatic potential in the complex only polar, neutral amino acid residues were selected.

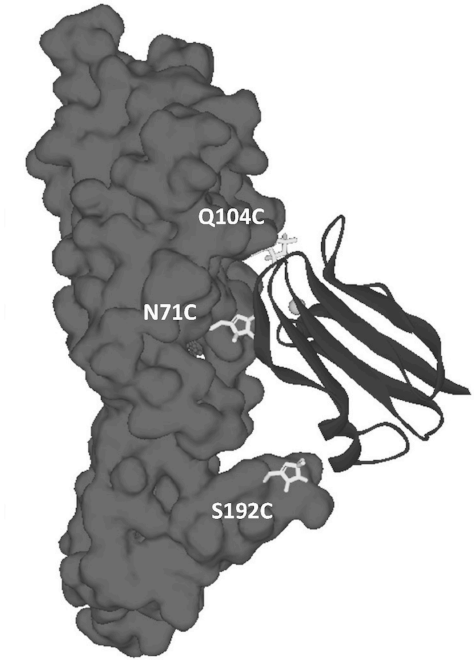

Figure 2.1. Location of the spin labels used in this study on the *Nostoc sp.* PCC 7119 Pc-Cyt *f* complex (PDB entry 1TU2, model 1[133]). Pc is shown in ribbons with the copper as a sphere. Cyt *f* is shown as surface. The spin labels were modeled on the structure and are shown as sticks.

Pc was produced in a cytoplasmic expression system (see the Experimental Section) in the ^{15}N enriched form with a Zn^{II} ion in the copper binding site to eliminate the paramagnetic effect of Cu^{II} and possible interference from electron transfer reactions.[134] To establish whether the introduction of a probe interferes with the Pc-Cyt *f* interaction, chemical shift analyses were carried out for all variants. First, Zn-substituted ^{15}N Pc was titrated with wt Cyt *f* and HSQC spectra were acquired

at each titration point. The binding constant was obtained by fitting the chemical shift perturbation curves for the most affected amide groups (Figure 2.2A), yielding K_D 8(3) x 10^{-5} M, similar to the reported values of 3.8 (0.1) x 10^{-5} M for Zn-Pc[135] and 6.2(0.9) x 10^{-5} M for Cd-substituted Pc.[135]

Also the binding map is similar, with the largest perturbations observed for the residues L14, G94 and A95, corresponding to the hydrophobic interaction patch, and H92 and R93, belonging to the basic patch (Figure 2.2B).

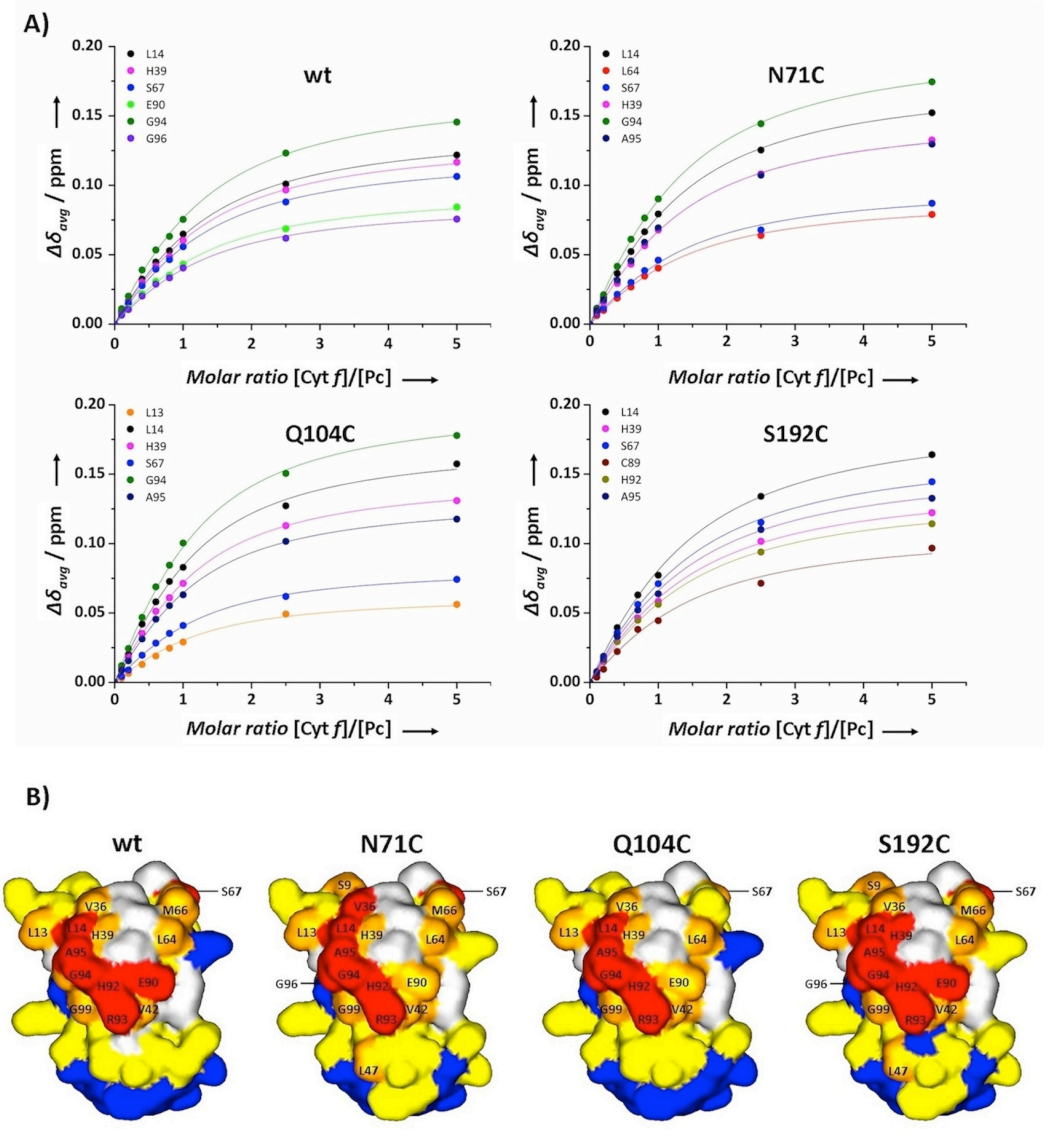

Figure 2.2. The interaction of *Nostoc* Zn-substituted Pc with wt Cyt *f* and MTS conjugated variants. A) Binding curves for selected residues were fitted globally to a 1:1 binding model (equation 2.1). B) Chemical shift perturbation maps of Zn-substituted Pc in the presence of wild type and MTS-conjugated Cyt *f*, colour-coded on a surface model of Pc (PDB-entry 2CJ3), with red, $\Delta\delta_{avg} \geq 0.10$ ppm; orange, $\Delta\delta_{avg} \geq 0.05$ ppm; yellow, $\Delta\delta_{avg} \geq 0.02$ ppm; blue, $\Delta\delta_{avg} < 0.02$ ppm. Prolines and residues with overlapping resonances are in grey.

Similar titrations of Pc and the cysteine mutants of Cyt *f* conjugated with the diamagnetic control label MTS yielded the dissociation constants listed in Table 2.1. The binding curves and maps are shown in Figure 2.2. Clearly, the mutation and attachment of MTS have very little effect on the affinity and the binding map.

Table 2.1. Dissociation constants of the complexes formed by *Nostoc* (Zn) Pc with wt and MTS-conjugated Cyt *f*. The errors are indicated in parentheses.

Cyt *f* mutant	K_D * 10^{-5} (M)
wild type	8 (3)
N71C-MTS	4 (1)
Q104C-MTS	3 (1)
S192C-MTS	4 (1)

Paramagnetic relaxation enhancements of Pc nuclei

The aim of this study was to gather distance restraints from PREs to refine the published solution structure. The residues selected for mutation to cysteine and tagging with the spin label are located around binding site for Pc on Cyt *f* in the solution structure model. The spin labels at these positions are thus expected to yield PRE of nuclei on different sides of Pc. For this purpose, the spin label MTSL was attached to the three Cyt *f* mutants and the tagged protein was added to Pc to a Cyt *f*/Pc molar ratio of 0.3. Under these conditions, the fraction of bound Pc is 24%. Large PREs were observed already at this ratio for numerous Pc amide groups with each variant of Cyt *f*-MTSL, illustrated in Figure 2.3.

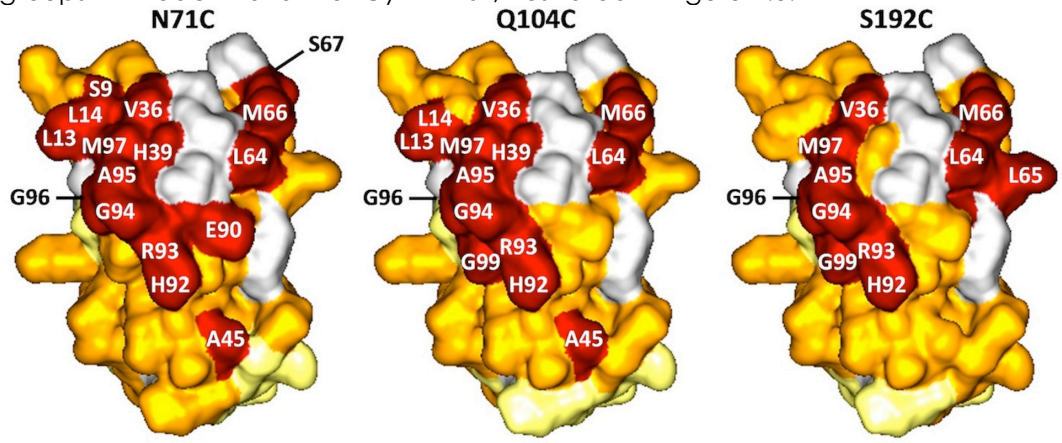

Figure 2.3. PRE maps of Zn-substituted Pc bound to MTSL-conjugated Cyt *f*, colour-coded on a surface model of Pc (PDB-entry 2CJ3) according to the three classes of restraints defined for the docking: red corresponds to residues with $I_p/I_d<0.10$; orange to $0.10<I_p/I_d<0.95$ and yellow to $I_p/I_d>0.95$. Prolines and residues with overlapping resonances are in grey.

Some resonances were broadened beyond detection. It is clear from the Cyt *f*

titrations that Pc binding is in the fast exchange regime, so an observed PRE is a weighted average of free Pc (no PRE), the encounter state (the AB* ensemble) and the final complex, AB, (Equation 2.5).

$$PRE_{obs} = f_1^{\text{free Pc}} \times 0 + f_2^{AB^*} \langle PRE \rangle^{AB^*} + f_3^{AB}\, PRE^{AB} \qquad f_1 + f_2 + f_3 = 1 \qquad (2.5)$$

The fraction of the free Pc (f_1) is 0.76 and that of bound Pc (f_2+f_3) is 0.24. By dividing the observed PRE by 0.24, the PRE for 100% bound Pc is obtained. These extrapolated PREs are plotted in Figure 2.4 (green symbols) against the Pc residue number.

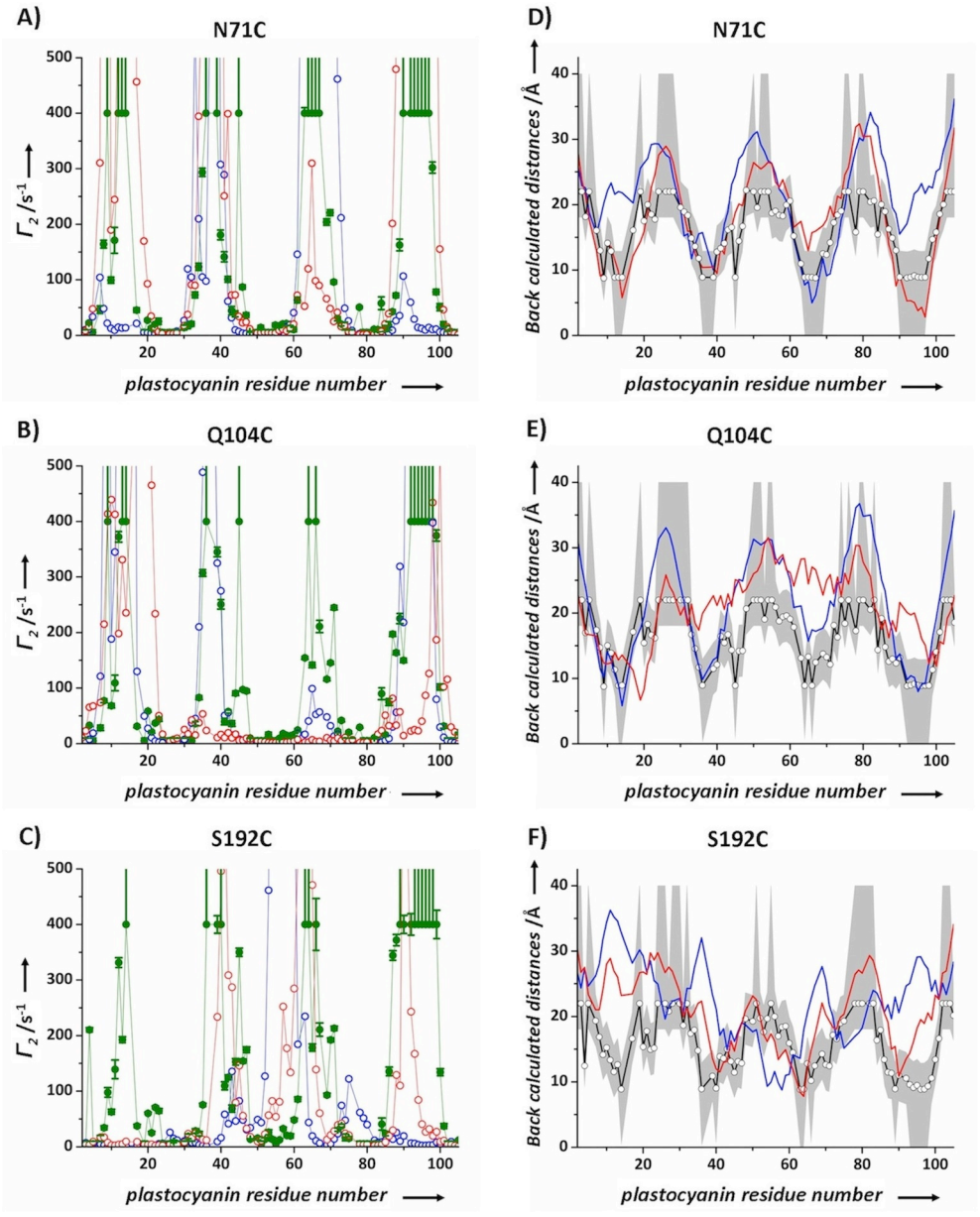

Figure 2.4. Left panel (A-C), observed and predicted PRE values for amide protons in Pc bound to MTSL conjugated Cyt *f* variants N71C (A), Q104C (B) and S192C (C). The observed PREs were extrapolated to represent the 100% bound state of Pc (green dots). PREs at 400 s^{-1} represent lower limits. The PREs calculated from the NMR solution structure based on PCS (PDB entry 1TU2, model 1[133]) are shown as blue symbols. The PREs calculated from the NMR solution structure based on PREs are shown as red symbols. Right panel (D-F), experimental and back calculated distances between Pc amide protons and MTSL conjugated Cyt *f* variants N71C (D), Q104C (E) and S192C (F). The white circles and black line represent the distances calculated from the experimental PREs (which were extrapolated to 100% bound Pc), where the grey area indicates the error margins. The distances derived from the NMR solution structure based on PREs are shown as a red line. The distances derived from the NMR solution structure based on PCS (PDB entry 1TU2, model 1[133]) are shown as a blue line.

Strikingly, the patterns are qualitatively similar for the three spin label positions, indicating that the same patches of Pc are strongly affected. When the fraction of AB* is neglected ($f_2 \approx 0$), the PRE can be predicted from the model of the final complex. Using model 1 of PDB entry 1TU2, the PRE^{AB} values were predicted for each amide in Pc (Figure 2.4, blue symbols). Clearly, the model alone cannot account for the observed PREs. Also, docking calculations were performed using distances derived from the PREs as restraints. Apart from a van der Waals repel function to avoid steric collisions no other interactions were included. The ensemble of the ten best structures is shown in Figure 2.5 and compared with the model based on PCS. In both cases Pc is bound in the region close to the haem, but the orientation differs. However, also the PRE-based model on its own cannot account for the observed PREs and the back calculated distances (Figure 2.4, red symbols in the left panel and red line in the right panel, respectively).

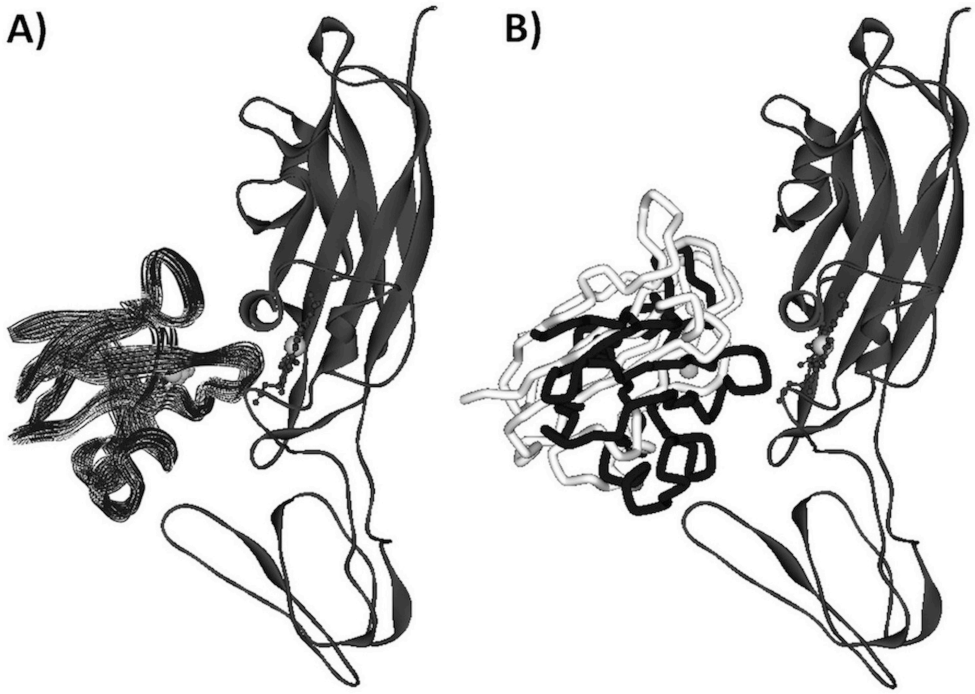

Figure 2.5. A) Model of the Pc-Cyt *f* complex obtained with PREs restraints. Cyt *f* is shown in ribbons and Pc as Cα trace. The ten lowest energy structures are visualized. B) Overlay of the orientations of Pc in the NMR solution structure based on PREs (shown as black Cα trace) and the NMR solution structure based on PCS (PDB entry 1TU2, model 1 [133], light grey).

Thus, it can be concluded that a single orientation is insufficient to describe the Pc-Cyt *f* complex. It is now well-established that PREs are very sensitive to lowly populated states. The poor fit between the PRE data and the modelled structure indicates that other orientations of Pc within the complex contribute to the PRE data. This conclusion is also borne out by the similarity of the PRE maps in Figure 2.3 for the Cyt *f* variants. If the Pc were in a single orientation in the complex, different patches of Pc residues would have been affected by PRE, because the spin labels are located around the binding site (see, for example, the red symbols in Figure 2.4). Yet, for each spin label position the same Pc surface region was affected by PREs, this also matches the side with the largest chemical shift perturbations. These observations suggest that Pc samples a large area of the surface of Cyt *f* with its hydrophobic patch. Our results are in accord with kinetic experiments,[121,122] which indicated that the interaction site of Pc depends on a few specific residues, whereas for Cyt *f* the residues relevant in the association are more spread over the protein surface. The formation of the encounter complex reduces the dimensionality of the diffusional search for the binding site that enables rapid ET.[21] It has been suggested that the population balance between the encounter state and the well-defined state depends on whether rapid ET can occur in encounter state orientations.[28] In complexes of small proteins the redox centres can get sufficiently close for ET in many of the protein orientations, but in larger complexes fast ET can only occur through certain areas of the protein surface, requiring the formation of a well-defined complex. Both Cyt f and Pc have an elongated shape and the metal is close to only a small part of the surface. Thus, it seems likely that a degree of specificity in the interaction is required in this complex to be active. Earlier studies suggested that the degree of dynamics varies between Cyt *f*/Pc complexes. Those of *P. laminosum*[54] and *Pr. hollandica*[32] appeared to be particularly dynamic. From the data presented in this study the fraction of the encounter complex cannot be established, but it is clear that it is significant, even though the complex from *Nostoc* would be categorized as well-defined given the earlier NMR data, the intermolecular PCS from the Cyt *f* haem to Pc.[120] Both PCS and PRE are sensitive to minor states populating the encounter complex in the case that the minor state experiences a much stronger paramagnetic effect than the major state. In the opposite case, when the major orientation is most affected by the paramagnetism, the presence of minor states may well go unnoticed, because it only leads to a small reduction of the observed effect. Here, the PCSs are large in particular for the major state, close to the paramagnetic haem, whereas the PREs will be dominated by those orientations that bring the nucleus close to the spin label, and thus, the PREs describe better the combination of the final complex and the encounter ensemble. Therefore, a good fit of the PCS data could be obtained with a single structure in the study of Diaz et al.,[120] while the same structure is insufficient to account for all PREs. More extensive spin labelling covering a large area of the surface will enable a detailed description of the encounter complex, as was shown for the ET complex of Cyt *c* and CcP.[28] Such experiments are presented in Chapter III.